Lippmann-Schwinger integral equation approach to the emission of radiation by sources located inside finite-sized dielectric structures

Søndergaard, T.; Tromborg, Bjarne

Published in:
Physical Review B (Condensed Matter and Materials Physics)

Link to article, DOI:
10.1103/PhysRevB.66.155309

Publication date:
2002

Document Version
Publisher's PDF, also known as Version of record

Lippmann-Schwinger integral equation approach to the emission of radiation by sources located inside finite-sized dielectric structures

T. Søndergaard*
Micro Managed Photons A/S, Institute of Physics, Aalborg University, Pontoppidanstræde 103, DK-9220 Aalborg Ø, Denmark

B. Tromborg†
Research Center COM, Technical University of Denmark, Building 345, DK-2800 Lyngby, Denmark
(Received 30 January 2002; revised manuscript received 7 May 2002; published 4 October 2002)

A full-vectorial integral equation method is presented for calculating near fields and far fields generated by a given distribution of sources located inside finite-sized dielectric structures. Special attention is given to the treatment of the singularity of the dipole source field. A method is presented for removing the dipole source field singularity from the integral equations to be solved. It is also shown how the numerical task can be reduced in the case of structures with cylindrical symmetry. The methods are applied to calculate the near fields, far fields, and the emission rate of light from a dipole source located in the center of a cylindrically symmetric dielectric disk. The emission for certain disk diameters, where a resonance condition is fulfilled, is enhanced by 13 times as compared to the emission from the same dipole source located in free space. The methods have prospective uses for analyzing the emission of light by sources in some antennas and optical components such as vertical cavity surface emitting lasers, microdisk lasers, and light emitting diodes. The methods also have prospective uses in quantum electrodynamics for studies of spontaneous emission from, e.g., an excited atom located inside a dieletric structure.

DOI: 10.1103/PhysRevB.66.155309 PACS number(s): 03.50.De, 02.30.Rz

I. INTRODUCTION

A Lippmann-Schwinger type integral equation has been used in astrophysics to model the scattering of light incident on dielectric grains and particles of various shapes in three dimensions.[1–5] This type of integral equation has also been used to calculate the near fields in a situation where a plane wave or a laser beam is incident on a microstructured dielectric surface.[6–11] By measuring the near fields in such a situation images can be created of the microstructure itself, and images can also be made of the fields in the microstructure.[13–15]

In near field optics a typical situation is to illuminate a dielectric structure from the outside and investigate the scattered field in a plane above the structure.[6] In this case the light source generating the incident beam of light is located outside the dielectric structure of interest. The incident beam of light is given, or equivalently, the distribution of sources generating the incident beam of light is given.

It is also possible to calculate the electric field inside the dielectric structure, and the dielectric structure is often referred to as the source region (see, e.g., Refs. 12 and 6 and references therein). The terminology of source region arises from a procedure where the dielectric structure is discretized into a number of small polarizable volume elements. Each element can be thought of as being equivalent to a dipole source with a polarization proportional to the field at the dipole position generated by all other sources. These dipole sources being driven by an external field are basically accounting for the response of a dielectric structure when the dielectric structure is illuminated by an electromagnetic field. Calculating the polarization of these driven dipole sources is equivalent to calculating the electric field inside the structure. In this paper we will also consider the field inside a dielectric structure, but this field is in part related to a type of sources that should not be considered a part of the usual source region terminology. In this paper we will consider the case of a given distribution of sources located inside a finite-sized dielectric structure. The polarization of a given dipole source is fixed in the same way that the incident beam of light and associated sources are fixed in previous work.[6] With a given distribution of sources located inside a dielectric structure, the structure is not illuminated from the outside, but is illuminated by sources located inside the structure itself. The dielectric structure can also in this case be thought of as a collection of sources that are driven by both the given sources and all other driven sources. The usual numerical procedure for solving the Lippmann-Schwinger integral equation relies on the assumption that the electric field within small volume elements is constant. This assumption becomes problematic in the case of a given source, such as the dipole, with an associated singular field. Singular electromagnetic fields and sources have previously been considered by van Bladel.[34] Further development of existing integral equation methods is necessary to enable the treatment of, in particular, the singularity of the field of a given dipole source, when the dipole is located inside a finite-sized dielectric structure. This is the scope of the present paper. The method will be exemplified for the case of a given dipole located in the center of a dielectric disk with finite radius.

The motivation for developing a method, which is capable of the treatment of given sources located inside a dielectric structure, is that this will be useful for modeling of antennas and a variety of light-emitting devices, such as light-emitting diodes and vertical cavity surface emitting lasers. In these devices the emission of radiation is related to a distribution of sources located inside the structure. Note that the dielectric disk we will consider is a basic building block in, e.g., the vertical cavity surface emitting laser and the microdisk laser.[16,17]

The method may also have prospective uses for modeling of the quantum electrodynamic properties of dielectric media. It was suggested already in 1946 by Purcell[32] that the rate of spontaneous emission can be modified indirectly via the electromagnetic properties of the structure in which the emitter is placed. An explanation is that a dielectric environment can modify the strength and distribution of electromagnetic modes with which the emitter can interact. The study of the emission of radiation from a given electric dipole source has been widely used to model enhancement and reduction in the rate of spontaneos emission from, e.g., an excited two-level atom.[16–30,18,31] For an electric dipole emitter located in a passive dielectric environment the total rate of emission is revealed both from the near field at the dipole position and from the integrated Poynting vector flux in the far field.[29] The Lippmann-Schwinger integral equation can be used to calculate the total emission associated with the given dipole using both near fields and far fields. The method presented in this paper therefore provides an additional method for approaching the calculation of (spontaneous) emission of radiation for emitters located inside general finite-sized dielectric structures.

The approach that will be presented for the treatment of a given distribution of sources can generally be applied to all kinds of finite-sized dielectric structures. However, we will consider a dielectric structure with cylindrical symmetry, namely, the dielectric disk, which can be modeled without supercomputing facilities. The Lippmann-Schwinger integral equation will be rewritten in a form where cylindrical symmetry is taken advantage of.[33] Essentially, the numerical problem, where the fields and the structure are discretized in three dimensions, will be reduced to several problems, one for each angular momentum component of the field, where the fields and the structure are discretized in only two dimensions. A number of tests of the method for taking advantage of cylindrical symmetry will be presented so that the method can be compared to previous methods[2,35] that do not take advantage of cylindrical symmetry.

The paper is organized in the following way. In Sec. II the method is presented for calculating near fields and far fields generated by given sources located inside finite-sized dielectric structures. In Sec. III it is shown how the numerical task can be reduced in the case of structures with cylindrical symmetry. The method for cylindrically symmetric structures is tested against analytic and numerical results. The methods are applied to the case of a given dipole source located inside a cylindrically symmetric dielectric disk in Sec. IV. The conclusion is given in Sec. V.

II. METHOD FOR CALCULATING NEAR FIELDS AND FAR FIELDS GENERATED BY SOURCES LOCATED *INSIDE* DIELECTRIC STRUCTURES

In this section a full-vectorial integral equation method is presented for calculating near fields and far fields generated by a given distribution of current sources located inside finite-sized dielectric structures. Special attention is given to the treatment of the dipole source field singularity.

The finite-sized dielectric structures considered in this paper are placed in a reference medium with known properties described by a Green's tensor. The finite-sized dielectric structure can be thought of as a scattering object in the reference medium. Scattering of light by dielectric structures with general geometries may be calculated using a Lippmann-Schwinger type integral equation of the form

$$\mathbf{E}(\mathbf{r})=\mathbf{E}^0(\mathbf{r})+\int \mathbf{G}(\mathbf{r},\mathbf{r}';1)\cdot k_0^2(\boldsymbol{\varepsilon}(\mathbf{r}')-\mathbf{I})\cdot\mathbf{E}(\mathbf{r}')d^3r', \tag{1}$$

where $\mathbf{I}$ is the unit tensor, $\mathbf{r}$ and $\mathbf{r}'$ are position coordinates, and $\mathbf{E}^0$ is a field solution in the case without the scattering object. The scattering object is introduced via the dielectric tensor $\boldsymbol{\varepsilon}(\mathbf{r})$, and since we consider free space as the reference medium, $\boldsymbol{\varepsilon}(\mathbf{r})-\mathbf{I}$ represents the change introduced in the reference medium by the presence of the scattering object. The retarded dyadic Green's tensor $\mathbf{G}(\mathbf{r},\mathbf{r}';1)$ describes the scattering properties of the reference medium free space, and k_0 is the free space wave number. The field $\mathbf{E}$ is a field solution for the case where the scattering object is present in the reference medium. The Green's tensor for a homogeneous dielectric with refractive index n will in this paper be written as $\mathbf{G}(\mathbf{r},\mathbf{r}';n)$. The reason for using a notation with the refractice index as an argument in the homogeneous medium Green's tensor is that we will need homogeneous medium Green's tensors both for the case of free space ($n=1$) and for another medium, e.g., GaAs, where the refractive index $n\neq 1$. The homogeneous medium Green's tensor is given by (see, e.g., Refs. 34 and 12)

$$\mathbf{G}(\mathbf{r},\mathbf{r}';n)=\left(\frac{1}{k_0^2n^2}\boldsymbol{\nabla}\boldsymbol{\nabla}+\mathbf{I}\right)g(\mathbf{r},\mathbf{r}';n). \tag{2}$$

The scalar homogeneous medium Green's function is defined by

$$g(\mathbf{r},\mathbf{r}';n)=\frac{e^{ik_0n|\mathbf{r}-\mathbf{r}'|}}{4\pi|\mathbf{r}-\mathbf{r}'|}. \tag{3}$$

In previous work (see, e.g., Refs. 1,2,35,3) the incident wave $\mathbf{E}^0(\mathbf{r})$ is a plane wave or another beam of light incident upon the scattering object from the outside. The incident wave $\mathbf{E}^0(\mathbf{r})$ is typically a solution to the homogeneous wave equation without sources involved. However, it is also possible to consider scattering of fields generated by sources, and in that case $\mathbf{E}^0$ is the field that these sources would have generated if the scattering object was not present, i.e.,

$$\mathbf{E}^0(\mathbf{r})=i\omega\mu\int \mathbf{G}(\mathbf{r},\mathbf{r}';1)\cdot\mathbf{J}(\mathbf{r}')d^3r', \tag{4}$$

where $\mathbf{J}(\mathbf{r})$ is the distribution of currents generating the field, ω is the angular frequency, and μ is the vacuum permittivity. The use of fields generated by a given distribution of currents is interesting for modeling of antennas and various types of light-emitting optical components.

In the numerical procedure used for solving the Lippmann-Schwinger type integral equation (1) it is common to discretize the structure in a number of volume elements

and assume constant fields within each volume element.[1,35,2,3] The necessary assumption of constant fields within discretization elements was the main reason for placing a dipole source outside the dielectric structure in our previous work,[33] as this assumption is problematic for highly singular fields. In this paper we will show how the integral equation (1) can be rewritten in a form where the singularity of the dipole field is removed. By removing the singularity from the integral equation it becomes feasible to calculate near and far fields generated by highly localized current distributions, such as dipole currents, when the currents are located inside the scattering object.

The electric field $\mathbf{E}(\mathbf{r})$, generated by a given dipole source located at position $\mathbf{r}_0$ in a dielectric structure with dielectric tensor $\boldsymbol{\varepsilon}(\mathbf{r})$, is given in terms of the dyadic Green's tensor $\mathbf{G}(\mathbf{r},\mathbf{r}_0)$ of the structure, i.e.,

$$\mathbf{E}(\mathbf{r}) = \omega^2 \mu \mathbf{G}(\mathbf{r},\mathbf{r}_0)\cdot\mathbf{d}, \tag{5}$$

where $\mathbf{d}$ is the dipole moment of the dipole source. The Green's tensor $\mathbf{G}(\mathbf{r},\mathbf{r}_0)$ contains all scattering properties of the combined system of scattering object and the reference medium. The Green's tensor is a solution to the following integral equation:

$$\mathbf{G}(\mathbf{r},\mathbf{r}_0) = \mathbf{G}(\mathbf{r},\mathbf{r}_0;1) + \int \mathbf{G}(\mathbf{r},\mathbf{r}';1)\cdot k_0^2(\boldsymbol{\varepsilon}(\mathbf{r}')-\mathbf{I})\cdot\mathbf{G}(\mathbf{r}',\mathbf{r}_0)d^3r'. \tag{6}$$

Also in this case, if we discretize the structure we cannot assume that $\mathbf{G}(\mathbf{r},\mathbf{r}_0)$ is constant within each discretization element due to the singularity of the Green's tensor at $\mathbf{r}=\mathbf{r}_0$. However, if the position $\mathbf{r}_0$ corresponds to a position with dielectric constant $\varepsilon = n^2$, and the dielectric constant is constant in the immediate vicinity of $\mathbf{r}_0$, then the Green's tensor can conveniently be written as the sum of two terms, where the first term is the Green's tensor for a homogeneous medium with refractive index n, and the second term $\mathbf{G}^{sc}$ is a scattering term that does not contain singularities, i.e.,

$$\mathbf{G}(\mathbf{r},\mathbf{r}_0) = \mathbf{G}(\mathbf{r},\mathbf{r}_0;n) + \mathbf{G}^{sc}(\mathbf{r},\mathbf{r}_0). \tag{7}$$

By inserting the expression (7) into Eq. (6) we obtain an integral equation for the scattering term, i.e.,

$$\mathbf{G}^{sc}(\mathbf{r},\mathbf{r}_0) = \mathbf{G}^{b}(\mathbf{r},\mathbf{r}_0) + \int \mathbf{G}(\mathbf{r},\mathbf{r}';1)\cdot k_0^2(\boldsymbol{\varepsilon}(\mathbf{r}')-\mathbf{I})\cdot\mathbf{G}^{sc}(\mathbf{r}',\mathbf{r}_0)d^3r', \tag{8}$$

where

$$\mathbf{G}^{b}(\mathbf{r},\mathbf{r}_0) = \mathbf{G}(\mathbf{r},\mathbf{r}_0;1) - \mathbf{G}(\mathbf{r},\mathbf{r}_0;n) + \int \mathbf{G}(\mathbf{r},\mathbf{r}';1)\cdot k_0^2(\boldsymbol{\varepsilon}(\mathbf{r}')-\mathbf{I})\cdot\mathbf{G}(\mathbf{r}',\mathbf{r}_0;n)d^3r'. \tag{9}$$

The electric field generated by a dipole source can similarly be written in the form

$$\mathbf{E}(\mathbf{r}) = \omega^2 \mu \mathbf{G}(\mathbf{r},\mathbf{r}_0;n)\cdot\mathbf{d} + \mathbf{E}^{sc}(\mathbf{r}), \tag{10}$$

and the corresponding integral equation for the scattered electric field becomes

$$\mathbf{E}^{sc}(\mathbf{r}) = \mathbf{E}^{b}(\mathbf{r}) + \int \mathbf{G}(\mathbf{r},\mathbf{r}';1)\cdot k_0^2(\boldsymbol{\varepsilon}(\mathbf{r}')-\mathbf{I})\cdot\mathbf{E}^{sc}(\mathbf{r}')d^3r', \tag{11}$$

where

$$\mathbf{E}^{b}(\mathbf{r}) = \omega^2 \mu \mathbf{G}^{b}(\mathbf{r},\mathbf{r}_0)\cdot\mathbf{d}. \tag{12}$$

The advantage of the integral equation (11) for the scattering term $\mathbf{E}^{sc}$ as compared to Eq. (1) is that $\mathbf{E}^{sc}$ is not singular, and consequently the assumption of constant scattered fields $\mathbf{E}^{sc}$ within small discretization elements is not problematic.

Before the new integral equation approach can be used it is necessary to first calculate the driving terms $\mathbf{G}^b$ and $\mathbf{E}^b$ which involve a volume overlap integral between two Green's tensors. The volume integral may involve integrating over a Green's tensor singularity at both positions $\mathbf{r}$ and $\mathbf{r}_0$. If these positions are far apart directly performing the volume integral is not problematic, but when $\mathbf{r}\approx\mathbf{r}_0$ performing directly the volume integral numerically requires a very high sampling density near the two singularities. Note that although there are several singular terms in the above expression (9) for $\mathbf{G}^b$ at $\mathbf{r}=\mathbf{r}_0$, the driving term $\mathbf{G}^b$ is not singular.

An appropriate method of handling the singularities in the driving terms is to transform the volume overlap integral Eq. (9) into a surface integral away from the singularity points $\mathbf{r}$ and $\mathbf{r}_0$. A further advantage is that the calculation of the surface integral is much faster than the calculation of the volume integral. Consider a dielectric structure of the form

$$\varepsilon(\mathbf{r}) = n^2, \quad \mathbf{r}\in V, \tag{13}$$

$$\varepsilon(\mathbf{r}) = 1, \quad \mathbf{r}\notin V. \tag{14}$$

We will also consider the case of a dipole placed at a position $\mathbf{r}_0$ inside the volume V, where the refractive index is n. All structures considered in this paper are of the form (13) and (14). In this case, the term $\mathbf{G}^b$ can be written in the form

$$\mathbf{G}^{b}(\mathbf{r},\mathbf{r}_0) = \mathbf{G}^{\partial V}(\mathbf{r},\mathbf{r}_0), \quad \mathbf{r}\in V, \tag{15}$$

$$\mathbf{G}^{b}(\mathbf{r},\mathbf{r}_0) = \mathbf{G}^{\partial V}(\mathbf{r},\mathbf{r}_0) - \mathbf{G}(\mathbf{r},\mathbf{r}_0;n), \quad \mathbf{r}\notin V, \tag{16}$$

where

$$\mathbf{G}^{\partial V}=\frac{n^2-1}{k_0^2 n^2}\int_{\partial V}\Big((\hat{n}\boldsymbol{\nabla}' g_1)\cdot(\boldsymbol{\nabla}'\boldsymbol{\nabla}' g_n) - (\hat{n}\cdot\boldsymbol{\nabla}' g_1)(\boldsymbol{\nabla}'\boldsymbol{\nabla}' g_n) - \frac{n^2}{n^2-1}(\hat{n}\cdot\boldsymbol{\nabla}' g_n)(\boldsymbol{\nabla}'\boldsymbol{\nabla}' g_1) + \frac{n^2}{n^2-1} g_n \hat{n}\cdot(\boldsymbol{\nabla}'\boldsymbol{\nabla}'\boldsymbol{\nabla}' g_1) - \mathbf{I}k_0^2\frac{n^2}{n^2-1}(g_1\hat{n}\cdot\boldsymbol{\nabla}' g_n - g_n\hat{n}\cdot\boldsymbol{\nabla}' g_1)\Big) dS'. \tag{17}$$

Here ∂V refers to the surface of the volume V, $\hat{n}$ is the surface outward normal vector, the prime denotes differentiation or integration with respect to the primed coordinates, and g_1, g_n are shorthand notation for the scalar homogeneous medium Green's functions $g_1=g(\mathbf{r},\mathbf{r}';1)$ and $g_n=g(\mathbf{r}',\mathbf{r}_0;n)$. A derivation of the expressions (15)–(17), which is also valid for gain materials, is rather lengthy and involves converting a number of volume integrals into surface integrals by use of the Green theorems. A derivation is given in the Appendix.

III. METHOD FOR TAKING ADVANTAGE OF CYLINDRICAL SYMMETRY

In the numerical procedure for solving the Lippmann-Schwinger integral equation the structure of interest is discretized into a number of volume elements in which the electric field can be assumed constant. Scattering of light by general three-dimensional objects has previously been investigated by, e.g., Purcell and Pennypacker,[1] Draine,[2] Martin *et al.*,[35] and Hoekstra *et al.*[3] by discretizing the dielectric structure of interest into cubic volume elements. For general three-dimensional scattering objects a large number of discretization elements is typically required in the numerical procedure.

For scattering objects with cylindrical symmetry it is possible to use another discretization scheme where the structure is discretized into ring volume elements.[33] All structures investigated in this paper have cylindrical symmetry. For completeness we will briefly present the method for taking advantage of cylindrical symmetry. Furthermore, the method will be tested against results obtained by discretizing into cubic volume elements.

For cylindrically symmetric structures it is convenient to expand the fields $\mathbf{E}$ and $\mathbf{E}^0$ in angular momentum components in the form

$$\mathbf{E}^m(\mathbf{r})=[\hat{z}E_z^m(\rho,z)+\hat{\rho}E_\rho^m(\rho,z)+\hat{\phi}E_\phi^m(\rho,z)]\exp(im\phi), \tag{18}$$

where $\hat{\rho}$, $\hat{\phi}$, $\hat{z}$ are the coordinate unit vectors, and ρ, ϕ, z are the coordinates in a cylindrical coordinate system. For structures with cylindrical symmetry there can be no coupling between field components with different angular momentum, and therefore only the component of $\mathbf{E}^0$ with a given angular momentum component m is needed for calculating the component of the total field $\mathbf{E}$ with the same angular momentum.

For a given angular momentum m it is sufficient to discretize the field components E_ρ^m, E_ϕ^m, E_z^m and the dielectric structure in ρ and z. Thereby the structure is actually discretized into ring volume elements. The numerical task of calculating the field at all points inside the three-dimensional object can be replaced by a series of tasks where the field is essentially calculated in two-dimensional planes. One calculation must be performed for each angular momentum component of the field. The field at all other points than those of the planes is obtained using symmetry considerations. For the case of a field $\mathbf{E}^0$ generated by a given distribution of sources placed near the axis of cylindrical symmetry it is sufficient to consider a very small number of angular momentum components m.

The Lippmann-Schwinger type integral equation (1) for cylindrically symmetric structures may be written

$$E_{p,i}^m-\sum_j\sum_{q,s=\rho,\phi,z} G_{pq,ij}^m k_0^2(\varepsilon_{qs}-\delta_{qs})E_{s,j}^m=E_{p,i}^{0,m}, \tag{19}$$

where the indices i,j refer to ring elements, the indices p,q,s refer to the field components in a cylindrical coordinate system, and

$$G_{pq,ij}^m=\int_{ringj}\hat{p}\cdot\mathbf{G}(\mathbf{r}_i,\mathbf{r}';1)\cdot\hat{q}'e^{im(\phi'-\phi_i)}d^3r', \tag{20}$$

where the coordinate ϕ_i, which also affects $\mathbf{r}_i$ and $\hat{p}$, can be arbitrary. A similar integral equation for the scattering term $\mathbf{E}^{sc}$ for cylindrically symmetric structures is obtained by replacing $E_{p,i}^m$ by $E_{p,i}^{sc,m}$ and replacing $E_{p,i}^{0,m}$ by $E_{p,i}^{b,m}$ in Eq. (19), where $E_{p,i}^{b,m}$ represents the angular momentum components of $\mathbf{E}^b$, and $E_{p,i}^{sc,m}$ is the angular momentum components of $\mathbf{E}^{sc}$.

In this paper we will consider a given dipole source located at the axis of cylindrical symmetry, the z axis, and the orientation of the dipole will be along the x axis, i.e., $\mathbf{d}=d\hat{x}$ ($\hat{x}=\hat{\rho}$ when $\phi=0$). In this case there are only two nonzero angular momentum components ($m=\pm1$) of the fields. The components $E_{\rho,i}^{b,\pm1}$, $E_{z,i}^{b,\pm1}$ are in this case directly related to $\mathbf{E}^b(\mathbf{r})$ when $\mathbf{r}$ is in the x-z plane. The components $E_{\phi,i}^{b,\pm1}$ are correspondingly related to $\mathbf{E}^b(\mathbf{r})$ when $\mathbf{r}$ is in the y-z plane.

The integrand in Eq. (20) is for $i=j$ integrated over the Green's tensor singularity. A convenient method of handling the singularity is again to convert the volume integral into a surface integral away from the singularity,[36] i.e.,

$$k_0^2 G_{pq,ii}^m=k_0^2\int_{ringi}\hat{p}\cdot\mathbf{G}(\mathbf{r}_i,\mathbf{r}';1)\cdot(\hat{q}'e^{im(\phi'-\phi_i)}-\hat{q})d^3r' - \delta_{pq}+\int_{\partial(ringi)}\hat{p}\cdot[-\mathbf{I}(\boldsymbol{\nabla}' g(\mathbf{r}_i,\mathbf{r}';1)\cdot\hat{n}) + \hat{n}\boldsymbol{\nabla}' g(\mathbf{r}_i,\mathbf{r}';1)]\cdot\hat{q}dS', \tag{21}$$

where the gradient is taken with respect to the primed coordinates, $\partial(ring\,i)$ refers to the surface of ring discretization element i, and $\hat{n}$ is the outward surface normal vector. Again the angle ϕ_i can be chosen arbitrarily when it is kept in mind that ϕ_i also affects $\mathbf{r}_i$, $\hat{p}$, and $\hat{q}$.

In the limit of ring elements with very small height and width the Green's tensor elements Eq. (21) can be approximated by analytic results of Yaghjian.[12] Using heights and widths that are so small that Yaghjian's results can be used directly is not practical. However, these analytic results are very useful for testing the calculation of $G_{pq,ii}$.

A strength of the Lippmann-Schwinger type integral equation methods is that the unknowns that have to be calculated to begin with can be restricted to the domain of the scattering object. After the field inside the scattering object is calculated, the field outside the scattering object is directly given from the field inside by use of the Lippmann-Schwinger type integral equation.

In the remaining part of Sec. III the integral equation method for structures with cylindrical symmetry will be tested against numerical results for scattering of a plane wave from a dielectric ring calculated by discretizing the ring in cubic volume elements. The method will also be tested against analytic results from Mie scattering theory. A similar comparison with Mie theory was presented by Draine[2] for cubic volume elements. We make a rough estimate of the reduction in the required number of discretization elements by comparing a calculation based on ring volume elements to the work of Draine based on cubic volume elements.

For the case of a plane wave incident on a dielectric sphere Mie scattering theory allows the calculation of, e.g., extinction and absorption efficiency factors Q_{ext}, Q_{abs}. These factors are defined by[2]

$$Q_{ext}=\frac{k_0}{|\mathbf{E}^0|^2}\int \mathrm{Imag}(\mathbf{E}^{0*}(\mathbf{r})\cdot[\boldsymbol{\varepsilon}(\mathbf{r})-\mathbf{I}]\cdot\mathbf{E}(\mathbf{r}))d^3r/\pi a^2, \tag{22}$$

$$Q_{abs}=\frac{k_0}{|\mathbf{E}^0|^2}\int \mathrm{Imag}(\mathbf{E}^{*}(\mathbf{r})\cdot[\boldsymbol{\varepsilon}(\mathbf{r})-\mathbf{I}]\cdot\mathbf{E}(\mathbf{r}))d^3r/\pi a^2, \tag{23}$$

where the incident plane wave is given by $\mathbf{E}^0(\mathbf{r})$, * represents the complex conjugate operation, and the resulting total electric field is given by $\mathbf{E}(\mathbf{r})$. The dielectric sphere, which is the scattering object, is introduced via the dielectric tensor $\boldsymbol{\varepsilon}(\mathbf{r})$. The radius of the sphere is given by a. The extinction and absorption efficiencies are measures of how efficiently light is lost from the incident beam of light due to scattering and absorption. For the case of a plane wave propagating along the z axis only $m=+1$ and $m=-1$ needs to be considered for the angular momentum because

$$\mathbf{E}^0(\mathbf{r})=\hat{x}E^0e^{ik_0z}=\left[\frac{1}{2}e^{i\phi}(\hat{\rho}+i\hat{\phi})+\frac{1}{2}e^{-i\phi}(\hat{\rho}-i\hat{\phi})\right]E^0e^{ik_0z}. \tag{24}$$

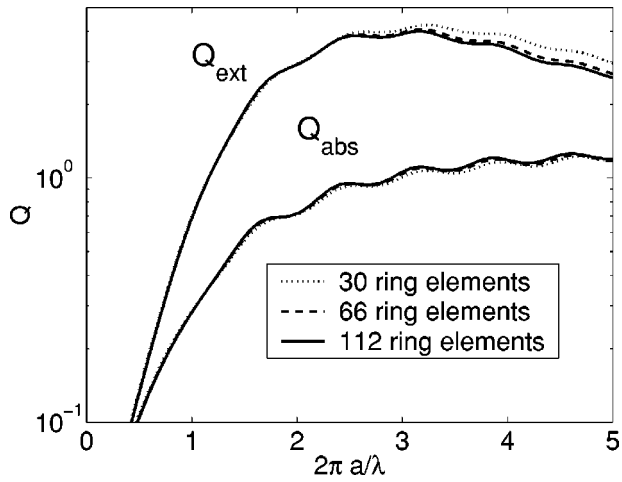

FIG. 1. Extinction and absorption efficiencies for a plane wave incident on a dielectric sphere with radius a and refractive index $1.7+i0.1$.

The numerical task is further simplified by the fact that the solution for the $m=-1$ field component can be obtained directly from the solution for the $m=1$ component by symmetry considerations. Therefore a numerical calculation is here only necessary for a single angular momentum component. Similarly, in the case of a dipole placed on the z axis and polarized along the x axis the field can be calculated by first solving for $m=1$ and then obtaining the corresponding solution for $m=-1$ by use of symmetry considerations.

Figure 1 shows the calculated extinction and absorption efficiencies for a plane wave incident on an absorbing dielectric sphere with refractive index $1.7+i0.1$ obtained using 30, 66, and 112 ring discretization elements. Effective medium theory has been applied to the boundary of the sphere to improve the representation of the dielectric sphere when the sphere is discretized.

This figure can be directly compared to a similar figure in Draine's work[2] where the sphere is discretized into cubic volume elements. By comparison, we obtain similar convergence using typically 20 times less discretization elements. It can be checked that the solid curves in Fig. 1 are very close to analytically calculated extinction and absorption efficiency factors obtained from Mie scattering theory. A ring element with a large radius will naturally replace more cubic volume elements than a ring element with a small radius. Because the volume elements are relatively close to the z axis the difference in required discretization elements is *only* on the order of a factor 20. We will now consider another example, namely, a dielectric ring, where the reduction in the number of discretization elements is significantly larger.

Consider a dielectric ring with height 15 nm, outer diameter 100 nm, and inner diameter 70 nm. The refractive index of the ring placed in free space is 3.6. This refractive index is representative of semiconductor materials such as GaAs at optical frequencies. The structure is cylindrically symmetric about the z axis. The ring is illuminated by a plane wave propagating along the z axis with the electric field polarized along the x axis. The wavelength of the incident field is 1000 nm. In Fig. 2 we show curves with constant field amplitude

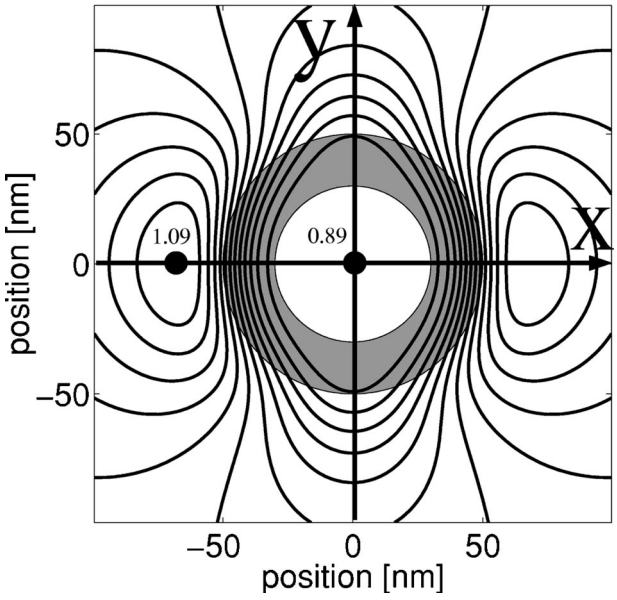

FIG. 2. Contour plot (linear scaling) of the amplitude of the electric field 20 nm below a dielectric ring normalized to the amplitude of the incident plane wave. The dielectric ring has outer diameter 100 nm, inner diameter 70 nm, and height 15 nm. The refractive index of the ring placed in free space is 3.6.

for the total field, being the sum of incident and scattered field, in a plane 20 nm below the dielectric ring. The difference in field amplitude between neighboring curves is kept constant (linear scaling). The minimum and maximum field amplitudes 0.89 and 1.09 have been indicated at two points marked with black filled circles. The shaded region in Fig. 2 shows the ring in the *x*-*y* plane. Figure 2 was calculated using nine ring resolution elements. The resolution in the ρ-*z* plane is therefore 5 nm$\times$5 nm.

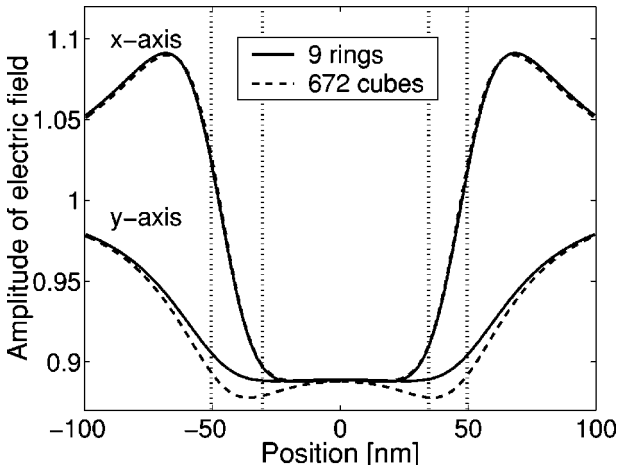

FIG. 3. Amplitude of the electric field 20 nm below a dielectric ring along the *x* axis and *y* axis. The ring is illuminated by a plane wave with unity electric field amplitude propagating along the *z* axis. The ring has outer diameter 100 nm, inner diameter 70 nm, and height 15 nm. The refractive index of the ring placed in free space is 3.6. The ring boundaries along the *x* axis and *y* axis are indicated with vertical dotted lines.

From symmetry considerations, the field in the entire *x*-*y* plane 20 nm below the dielectric ring can in fact be constructed from the field along the positive *x* axis and positive *y* axis in this plane. When the field is known along these two lines the field can be constructed at all other points in the plane by symmetry considerations. The amplitude of the field along the *x* axis and the *y* axis calculated using nine ring resolution elements is shown as the solid curve in Fig. 3. The boundaries of the dielectric ring in the *x*-*y* plane are indicated with vertical dotted lines. The dashed curve in Fig. 3 shows a similar calculation obtained by use of cubic volume elements with a corresponding resolution of 5 nm$\times$5 nm $\times$5 nm. In this case 672 volume elements were required for resolving the dielectric ring. This corresponds to more than 70 times the number of used ring resolution elements. For the ring elements, increasing the resolution to 36 points resulted in a difference of less than 0.001 for all positions in the *x*-*y* plane. This difference would hardly be visible in Fig. 3. The agreement between using cubic volume elements and ring elements is very good along the *x* axis, and reasonable along the *y* axis. In the present case the convergence obtained using ring volume elements is far better compared to cubic volume elements because the circular boundary of the ring is treated exactly with ring elements. When cubic volume elements are used it is more difficult to obtain a good representation of the cylindrical boundaries. However, as the number of cubic volume elements is increased, the result will converge to the result of the solid curve in Fig. 3.

IV. RESULTS FOR A DIPOLE SOURCE LOCATED INSIDE THE DIELECTRIC DISK

In this section the Lippmann-Schwinger integral equation method will be applied to the case of a given dipole source located in the center of a cylindrically symmetric dielectric disk. The results of this section have been obtained by using both the method for treating sources located inside dielectric structures (Sec. II), and the method for taking advantage of cylindrical symmetry (Sec. III). The dielectric disk is placed in free space. The axis of symmetry is the *z* axis. The dipole source is polarized along the *x* axis. The refractive index of the disk is 3.6. The height of the dielectric disk is $h = 150$ nm, and the emission wavelength is 1000 nm. The emission of radiation from the dipole will be investigated for various choices of the disk radius.

For a passive dielectric structure there are two methods for calculating the total emission of radiation from the dipole source. The first method is to integrate the Poynting vector flux through a closed surface surrounding the emitter. This is achieved by, e.g., integrating the emission per unit solid angle in the far field over all directions. The power flux of emitted light dP per unit solid angle $d\Omega$ in the far field is given by

$$\frac{dP}{d\Omega} = \Gamma(\theta,\phi) = \lim_{r\to\infty} r^2 |\mathbf{S}(\mathbf{r})|, \tag{25}$$

where θ and ϕ are angles that define the direction of the radius vector $\mathbf{r}$, and $\mathbf{S}$ is the Poynting vector, which for large distances $r = |\mathbf{r}|$ reduces to

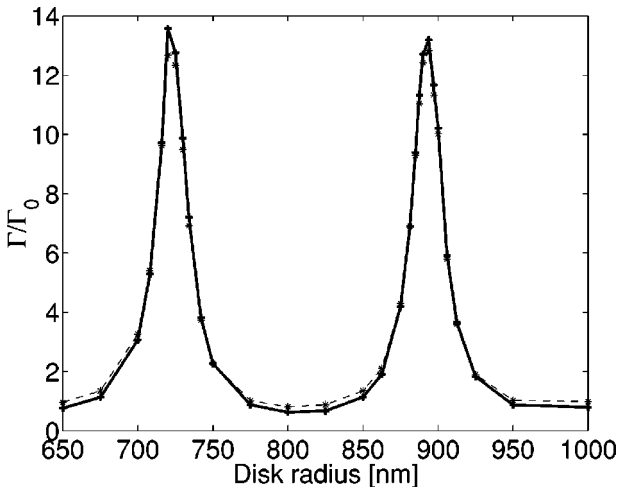

FIG. 4. Emission rate from a dipole source located in the center of a dielectric disk. The disk is placed in free space. The refractive index of the disk is 3.6, and the height is 150 nm. The emission wavelength is 1000 nm.

$$\mathbf{S}=2\frac{\mathbf{r}}{r}\varepsilon_0 c|\mathbf{E}(\mathbf{r})|^2. \tag{26}$$

Here c is the vacuum speed of light. The total emission of electromagnetic radiation per unit time from the dipole source can be obtained by integrating the emission per unit solid angle over all directions, i.e.,

$$\Gamma_{tot}=\int_{\phi=0}^{2\pi}\int_{\theta=0}^{\pi}\Gamma(\theta,\phi)\sin(\theta)d\theta d\phi. \tag{27}$$

Another method for obtaining the total emission of radiation from the dipole source in a passive dielectric structure is given by (see, e.g., Ref. 29)

$$\Gamma_{tot}=2\omega\,\mathrm{Imag}(\mathbf{d}\cdot\mathbf{E}(\mathbf{0})), \tag{28}$$

i.e., the total emission is proportional to the imaginary component of the electric field along the dipole orientation at the position of the dipole. Note that the expression (28) is not valid for active structures.[29] Notice that the real part of the electric field along the direction of the dipole is highly singular at the dipole position. The expression (28) can be evaluated by calculating the near field inside the dielectric structure at the position of the dipole. The methods presented in this paper can be used for calculating the total emission by use of both Eqs. (27) and (28). The total emission from the dipole source calculated by use of Eq. (27) as a function of the radius of the disk is shown as the solid curve in Fig. 4. The corresponding result obtained by using Eq. (28) is shown as the dashed curve. In both cases the total emission is normalized relative to the emission Γ_0 from the same dipole source located in free space. In the calculations presented in this section the dielectric disk has been discretized into ring volume elements with a height of approximately 17 nm and a width of 12.5 nm or smaller.

From Fig. 4 it is clear that the emission rate peaks for certain choices of the disk radius. The figure shows peaks in the emission rate around disk radii of 720 nm and 894 nm.

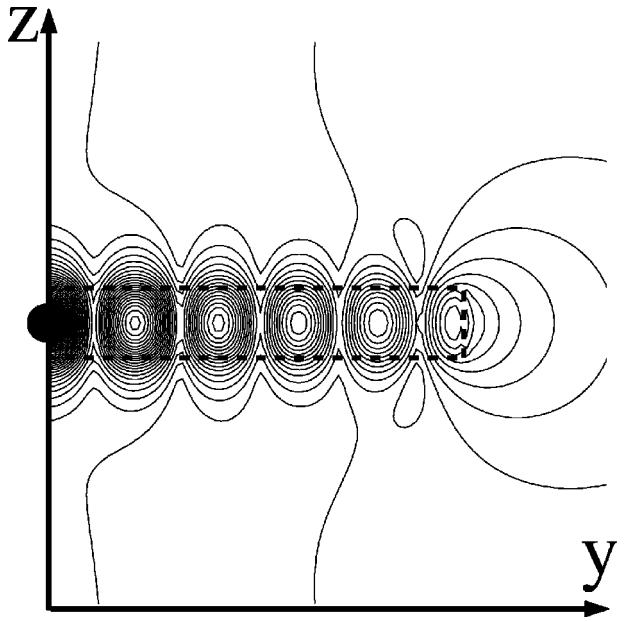

FIG. 5. Amplitude of electric field in the *z*-*y* plane generated by an electric dipole in the center of a cylindrically symmetric dielectric disk with height 150 nm, radius 894 nm, and refractive index 3.6. The boundary of the dielectric disk in the *y*-*z* plane is indicated with a dashed line. The axis of cylindrical symmetry is the *z* axis. The emission wavelength is 1000 nm, and the dipole indicated with a black filled circle is oriented along the *x* axis. Linear scaling has been used for the contour plot.

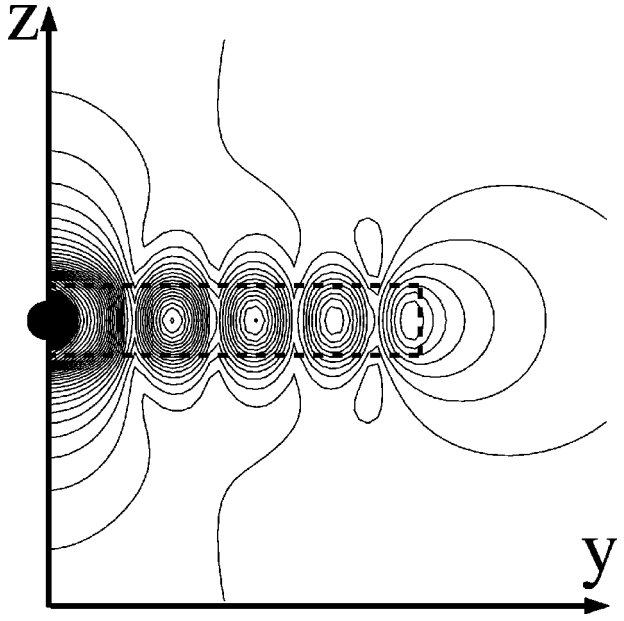

FIG. 6. Amplitude of electric field in the *z*-*y* plane generated by an electric dipole in the center of a cylindrically symmetric dielectric disk with height 150 nm, radius 800 nm, and refractive index 3.6. The boundary of the dielectric disk in the *y*-*z* plane is indicated with a dashed line. The axis of cylindrical symmetry is the *z* axis. The emission wavelength is 1000 nm, and the dipole indicated with a black filled circle is oriented along the *x* axis. Linear scaling has been used for the contour plot.

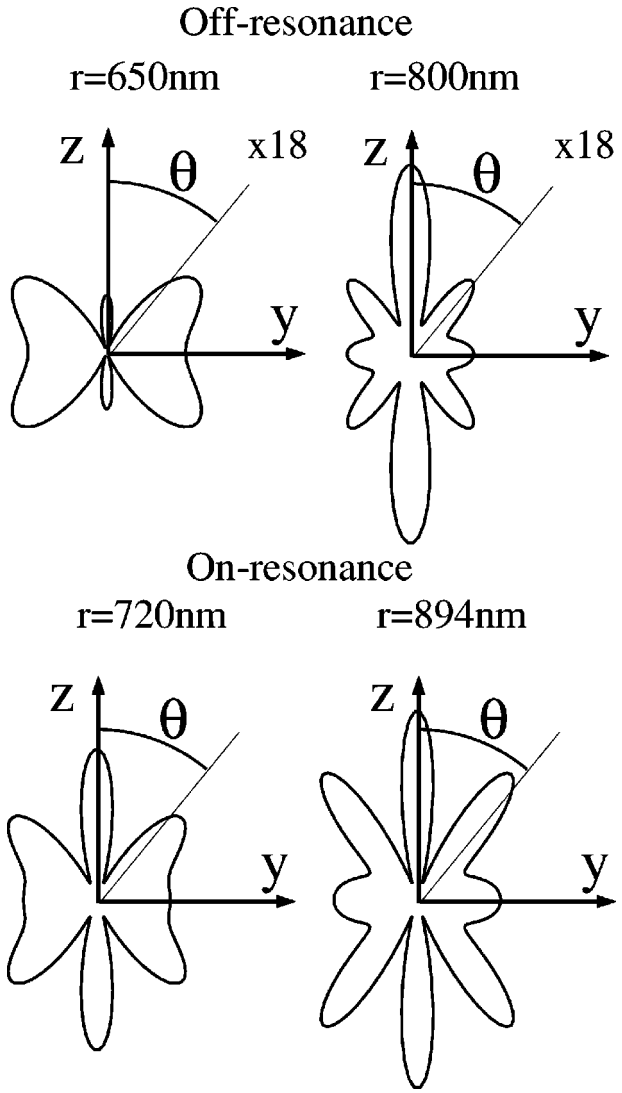

FIG. 7. Far-field angular emission patterns from a dipole source in the center of a cylindrically symmetric dielectric disk with height 150 nm, and refractive index 3.6. The axis of cylindrical symmetry for the structure is the *z* axis. The dipole is oriented along the *x* axis. The emission pattern is shown for the disk radii $r=650$ nm, 720 nm, 800 nm, and 894 nm.

The difference in disk radius for the two neighboring peaks corresponds roughly to half a wavelength in the media for the fundamental mode propagating in a slab waveguide with same height and refractive index as the dielectric disk. This indicates that the peaks are related to the excitation of standing wave resonance fields in the disk. The emission may be enhanced by a factor 13 as compared to the corresponding emission from the same dipole located in free space. The factor 13 is not large compared to, e.g., factors of around 300 found for dielectric microspheres (see, e.g., Refs. 26 and 27). An increase by a factor 5 has been measured for spontaneous emission from quantum dots in GaAs-based pillar microcavities, and an increase by a factor 15 has been measured for a microdisk.[28,37–39]

In general, whether or not a resonance condition is fulfilled resulting in a large rate of emission depends on both

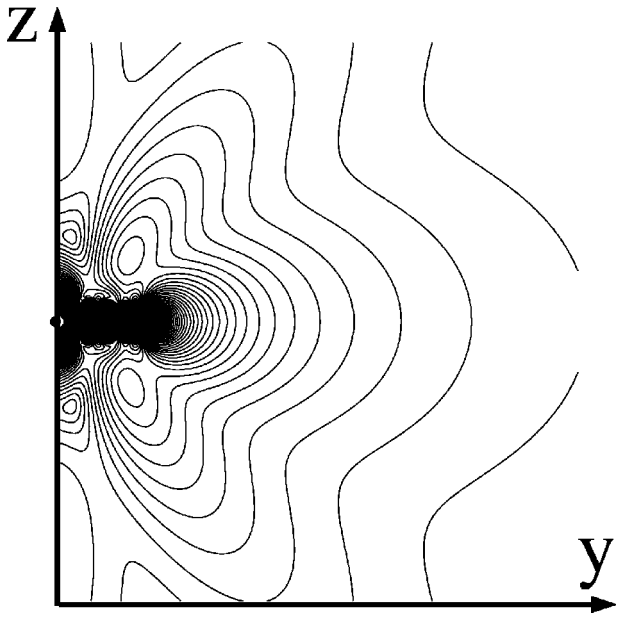

FIG. 8. Amplitude of electric field in the *z*-*y* plane generated by an electric dipole in the center of a cylindrically symmetric dielectric disk with height 150 nm, radius 800 nm, and refractive index 3.6. The axis of cylindrical symmetry for the disk is the *z* axis. The emission wavelength is 1000 nm, and the dipole is oriented along the *x* axis. Linear scaling has been used for the contour plot.

position, emission wavelength, and orientation of the dipole emitter in the dielectric structure. The difference in emission as the disk radius is varied also leads us to conclude that the emission can be very different for disks with a finite radius as compared to the disks with infinite radius investigated by other authors.[18,21–25,30,40]

Near fields on and off resonance are illustrated by constant field intensity curves in Figs. 5 and 6, respectively. The difference in field amplitude between neighboring contour curves is the same between all neighboring contour curves (linear scaling). The boundary of the dielectric disk is indicated with a dashed line. In Fig. 5 the amplitude of the electric field is shown for the disk radius 894 nm, where a resonance is seen in the total emission. The near field contour plot shows that there are standing wave type resonances both along the *z* axis and along the *y* axis in the disk. Along the *z* axis the height of the disk corresponds roughly to half a wavelength in the medium resulting in a half-wavelength type standing wave along the *z* axis. The diameter of the disk is several wavelengths in the medium, and standing waves give rise to nodes and antinodes in the total field amplitude along the *y* axis. The dipole is positioned exactly at the position of an antinode in the standing wave field pattern resulting in the large emission rate. When making the contour plot a small region was excluded around the dipole, indicated with a black filled circle, because the dipole field amplitude becomes singular at the dipole position. From the near field image at resonance (Fig. 5) we can from the periodicity of the standing wave pattern along the *y* axis estimate that half a wavelength in the media corresponds roughly to 175 nm, which is roughly equivalent to the distance between the two peaks in Fig. 4.

The similar situation is shown in Fig. 6 for the disk radius 800 nm. For this choice of disk radius we again observe a standing wave pattern in the near field both along the z axis and along the y axis. In this case the dipole is positioned at a node for the standing wave field pattern along the y axis. This is, however, not seen at first because the intensity still peaks in the center of the disk at the position of the dipole due to the dipole field singularity. Notice that compared to Fig. 5 the radius of the disk has been reduced by roughly one quarter wavelength in the media.

Some examples of far-field radiation patterns $\Gamma(\theta,\phi)$ are shown in Fig. 7 for four different choices of disk radius. The patterns show the emission per unit solid angle as a function of the off-axis angle θ for a fixed azimuthal angle ϕ. In this case we consider the z-y plane ($\phi=\pi/2$) as this is the plane in which the shape of the radiation patterns is most strongly affected by the presence of the dielectric disk. The similar radiation patterns for the z-x plane all resemble a figure 8, which would also be the shape of the radiation pattern for the dipole in free space for the z-x plane. The free space radiation pattern for the z-y plane is a circle, and it is therefore clear that the shapes of the radiation patterns in Fig. 7 are very different compared to the free space radiation pattern. The four far-field patterns can be compared in magnitude when it is taken into account that the amplitude of the far-field plots for the radius 650 nm and 800 nm have been multiplied with a factor 18 as compared to the results for radii 720 nm and 894 nm. Consider, for example, the far-field emission pattern for the radius 800 nm. In this emission pattern there are certain preferred directions for emission of radiation. These preferred directions of emission are not easily recognized from a near field image such as Fig. 6. A clear correspondence between the near field image and the far-field emission pattern becomes apparent when the near field image is extended to show the fields in distances of several free space wavelengths away from the dielectric disk. In Fig. 8 the near field for the radius 800 nm is shown for a large spatial region. In this case we obtain a clear correspondence between the preferred directions of propagation in both near field and far-field images.

V. CONCLUSION

In conclusion, a Lippmann-Schwinger type integral equation method has been presented for the treatment of sources located inside finite-sized dielectric structures. Special attention was given to the treatment of the dipole source field singularity. A method was presented for removing the dipole source field singularity from the Lippmann-Schwinger integral equation to be solved.

A Lippmann-Schwinger type integral equation method was, furthermore, presented for taking advantage of the symmetry in cylindrically symmetric structures. In this method the dielectric structure is discretized into ring volume elements. The method based on ring volume elements was tested and compared with a previous method that does not take advantage of cylindrical symmetry based on discretizing into cubic volume elements. Depending on the choice of dielectric structure we observed large reductions in the required number of discretization elements when taking advantage of cylindrical symmetry. For a dielectric sphere the reduction was on the order of a factor 20, and for a dielectric ring the reduction was on the order of a factor 70.

The methods were exemplified for the case of a given dipole source located in the center of a cylindrically symmetric dielectric disk. The total emission from the dipole source was investigated for various choices of the disk radius. Certain disk radii resulted in a high total emission of light from the dipole. In the case of high total emission of light a calculation of the near field revealed that the dipole was located at an antinode of a standing wave field pattern. The standing wave field pattern corresponds to a resonance field of the dielectric disk. At resonance, the total emission was enhanced by a factor 13 as compared to the emission from the same dipole located in free space. Near fields were also presented for the case of low total emission from the dipole. In that case the dipole was located at a node in a standing wave field pattern. Far fields were presented for choices of disk radius resulting in high and low emission of radiation.

ACKNOWLEDGMENTS

D. Lenstra and his group at Vrije Universiteit, Amsterdam, The Netherlands, are acknowledged for their hospitality during part of this work. The work was carried out while TS was with Research center COM, Technical University of Denmark.

APPENDIX: DERIVATION OF DRIVING TERM

In this appendix the following volume integral expression for $\mathbf{G}^b$:

$$\mathbf{G}^b(\mathbf{r},\mathbf{r}_0)=\mathbf{G}(\mathbf{r},\mathbf{r}_0;1)-\mathbf{G}(\mathbf{r},\mathbf{r}_0;n)+\int_V \mathbf{G}(\mathbf{r},\mathbf{r}';1)k_0^2(n^2-1)\cdot\mathbf{G}(\mathbf{r}',\mathbf{r}_0;n)d^3r' \tag{A1}$$

will be converted into a surface integral expression. Thereby a derivation will be presented for the expressions (15)–(17).

We will consider the case where both positions $\mathbf{r}$ and $\mathbf{r}_0$ are inside the volume V and convert the volume integral into a surface integral by use of the Green theorems. The Green theorems cannot be applied directly to a volume integral with singularities in the integrand. The integral directly over the singularities at $\mathbf{r}$ and $\mathbf{r}_0$ can be calculated by enclosing the singularities by infinitesimally small spherical volumes δV_1 and δV_n. Here δV_1 is a sphere around $\mathbf{r}$, and δV_n is a sphere around $\mathbf{r}_0$. When integrating over the spheres δV_1 and δV_n one of the two Green's tensors can be treated as constant for $\mathbf{r}\neq\mathbf{r}_0$. The integral of the other Green's tensor over the sphere has been tabulated by Yaghjian.[12] The contribution to Eq. (A1) from these small spheres is then given by

$$\int_{\delta V_1} \mathbf{G}(\mathbf{r},\mathbf{r}';1)k_0^2(n^2-1)\cdot\mathbf{G}(\mathbf{r}',\mathbf{r}_0;n)d^3r' = -\frac{1}{3}(n^2-1)\mathbf{G}(\mathbf{r},\mathbf{r}_0;n), \tag{A2}$$

$$\int_{\delta V_n} \mathbf{G}(\mathbf{r},\mathbf{r}';1)k_0^2(n^2-1)\cdot\mathbf{G}(\mathbf{r}',\mathbf{r}_0;n)d^3r' = -\frac{1}{3}\frac{n^2-1}{n^2}\mathbf{G}(\mathbf{r},\mathbf{r}_0;1). \tag{A3}$$

Before the Green theorems are applied the remaining integral is rewritten in a convenient form by use of the following Green's tensor relation:

$$\mathbf{G}(\mathbf{r},\mathbf{r}';n)=\frac{1}{k_0^2n^2}(\boldsymbol{\nabla}\boldsymbol{\nabla}-\mathbf{I}\nabla^2)g(\mathbf{r},\mathbf{r}';n), \quad \mathbf{r}\neq\mathbf{r}', \tag{A4}$$

where the scalar homogeneous medium Green's function g is defined in Eq. (3). The expression (A4) is obtained from Eq. (2) by use of the following property of the scalar homogeneous medium Green's function:

$$(\nabla^2+k_0^2n^2)g(\mathbf{r},\mathbf{r}';n)=-\delta(\mathbf{r}-\mathbf{r}'). \tag{A5}$$

In Eq. (A4) the differentiations could also be with respect to the primed coordinates. We will use g_1 as shorthand notation for $g(\mathbf{r},\mathbf{r}';1)$ and g_n as shorthand notation for $g(\mathbf{r}',\mathbf{r}_0;n)$. The remaining volume integral may then be written

$$\begin{aligned}\int_{V\setminus\{\delta V_1\cup\delta V_n\}} \mathbf{G}(\mathbf{r},\mathbf{r}';1)k_0^2(n^2-1)\cdot\mathbf{G}(\mathbf{r}',\mathbf{r}_0;n)d^3r' &= \frac{n^2-1}{k_0^2n^2}\int_{V\setminus\{\delta V_1\cup\delta V_n\}}[(\boldsymbol{\nabla}'\boldsymbol{\nabla}'g_1)\cdot(\boldsymbol{\nabla}'\boldsymbol{\nabla}'g_n)\\ &-(\boldsymbol{\nabla}'\boldsymbol{\nabla}'g_1)\nabla'^2g_n-(\boldsymbol{\nabla}'\boldsymbol{\nabla}'g_n)\nabla'^2g_1\\ &+\mathbf{I}(\nabla'^2g_1)(\nabla'^2g_n)]d^3r',\end{aligned} \tag{A6}$$

where the integral is over the volume V minus the volume regions δV_1 and δV_n. The integral can be transformed into a surface integral by use of the following formulas that we have derived using the Green theorems:

$$\begin{aligned}\int_{V'}(\boldsymbol{\nabla}'\boldsymbol{\nabla}'g_1)\cdot(\boldsymbol{\nabla}'\boldsymbol{\nabla}'g_n)d^3r' &= \int_{\partial V'}(\hat{n}\boldsymbol{\nabla}'g_1)\cdot(\boldsymbol{\nabla}'\boldsymbol{\nabla}'g_n)dS'\\ &-\int_{\partial V'}g_1\hat{n}\cdot(\boldsymbol{\nabla}'\boldsymbol{\nabla}'\boldsymbol{\nabla}'g_n)dS'\\ &+n^2\int_{V'}(\boldsymbol{\nabla}'\boldsymbol{\nabla}'g_n)\nabla'^2g_1d^3r',\end{aligned} \tag{A7}$$

$$\begin{aligned}\frac{n^2-1}{n^2}\int_{V'}(\boldsymbol{\nabla}'\boldsymbol{\nabla}'g_1)\nabla'^2g_nd^3r' &= \int_{\partial V'}(\hat{n}\cdot\boldsymbol{\nabla}'g_n)(\boldsymbol{\nabla}'\boldsymbol{\nabla}'g_1)dS'\\ &-\int_{\partial V'}g_n(\hat{n}\cdot\boldsymbol{\nabla}')(\boldsymbol{\nabla}'\boldsymbol{\nabla}'g_1)dS',\end{aligned} \tag{A8}$$

$$\begin{aligned}(1-n^2)\int_{V'}(\boldsymbol{\nabla}'\boldsymbol{\nabla}'g_n)\nabla'^2g_1d^3r' &= \int_{\partial V'}(\hat{n}\cdot\boldsymbol{\nabla}'g_1)(\boldsymbol{\nabla}'\boldsymbol{\nabla}'g_n)dS'\\ &-\int_{\partial V'}g_1(\hat{n}\cdot\boldsymbol{\nabla}')(\boldsymbol{\nabla}'\boldsymbol{\nabla}'g_n)dS',\end{aligned} \tag{A9}$$

$$\begin{aligned}\frac{n^2-1}{n^2}\int_{\partial V'}(\nabla'^2g_1)(\nabla'^2g_n)d^3r' &= -k_0^2\int_{\partial V'}(g_1\hat{n}\cdot\boldsymbol{\nabla}'g_n-g_n\hat{n}\cdot\boldsymbol{\nabla}'g_1)dS',\end{aligned} \tag{A10}$$

where $\hat{n}$ is the outward surface normal vector, and V' refers to a general volume where the integrands are nonsingular.

Thereby

$$\begin{aligned}\int_{V\setminus\{\delta V_1\cup\delta V_n\}} \mathbf{G}(\mathbf{r},\mathbf{r}';1)k_0^2(n^2-1)\cdot\mathbf{G}(\mathbf{r}',\mathbf{r}_0;n)d^3r' &= \frac{n^2-1}{k_0^2n^2}\int_{\partial(V\setminus\{\delta V_1\cup\delta V_n\})}\Bigg((\hat{n}\boldsymbol{\nabla}'g_1)\cdot(\boldsymbol{\nabla}'\boldsymbol{\nabla}'g_n)-(\hat{n}\cdot\boldsymbol{\nabla}'g_1)(\boldsymbol{\nabla}'\boldsymbol{\nabla}'g_n)-\frac{n^2}{n^2-1}(\hat{n}\cdot\boldsymbol{\nabla}'g_n)(\boldsymbol{\nabla}'\boldsymbol{\nabla}'g_1)\\ &+\frac{n^2}{n^2-1}g_n(\hat{n}\cdot\boldsymbol{\nabla}')(\boldsymbol{\nabla}'\boldsymbol{\nabla}'g_1)-\mathbf{I}k_0^2\frac{n^2}{n^2-1}(g_1\hat{n}\cdot\boldsymbol{\nabla}'g_n-g_n\hat{n}\cdot\boldsymbol{\nabla}'g_1)\Bigg)dS'.\end{aligned} \tag{A11}$$

Note that the surface integral here includes an integration over both the surface of the volume V but also an integration over the surface of the infinitesimally small volumes δV_1 and δV_n. The integrands in the surface integrals are highly singular near the surfaces of δV_1 and δV_n. The contribution from the surfaces around these singularities result in terms containing both Green's functions and second derivatives $(\nabla\nabla)$ of Green's functions.

A relatively simple integral over the surface of one of the small spheres is

$$\int_{\partial\delta V_1}(\hat{n}\nabla' g_1)\cdot(\nabla'\nabla' g_n)dS' \approx \int_{\partial\delta V_1}\frac{(\mathbf{r}'-\mathbf{r})(\mathbf{r}'-\mathbf{r})}{4\pi|\mathbf{r}'-\mathbf{r}|^4}dS'\cdot\nabla\nabla g(\mathbf{r},\mathbf{r}_0;n) \approx \frac{1}{3}\nabla\nabla g(\mathbf{r},\mathbf{r}_0;n). \tag{A12}$$

Here it was sufficient to include only the most singular terms in ∇g_1.

In a similar way we obtain

$$\int_{\partial\delta V_1}(\hat{n}\cdot\nabla' g_1)(\nabla'\nabla' g_n)dS' \approx \nabla\nabla g(\mathbf{r},\mathbf{r}_0;n), \tag{A13}$$

$$\int_{\partial\delta V_n}(\hat{n}\cdot\nabla' g_n)(\nabla'\nabla' g_1)dS' \approx \nabla\nabla g(\mathbf{r},\mathbf{r}_0;1), \tag{A14}$$

$$\int_{\partial\delta V_n}(\hat{n}\cdot\nabla' g_n g_1)dS' \approx g(\mathbf{r},\mathbf{r}_0;1), \tag{A15}$$

$$\int_{\partial\delta V_1}(\hat{n}\cdot\nabla' g_1 g_n)dS' \approx g(\mathbf{r},\mathbf{r}_0;n). \tag{A16}$$

In order to evaluate the other surface integrals it becomes necessary to make the following Taylor expansions:

$$g_n \approx g(\mathbf{r},\mathbf{r}_0;n)+(\mathbf{r}'-\mathbf{r})\cdot\nabla g(\mathbf{r},\mathbf{r}_0;n) +\frac{1}{2}(\mathbf{r}'-\mathbf{r})\cdot(\nabla\nabla g(\mathbf{r},\mathbf{r}_0;n))\cdot(\mathbf{r}'-\mathbf{r}), \quad \mathbf{r}'\approx\mathbf{r}, \tag{A17}$$

$$\nabla' g_n \approx \nabla g(\mathbf{r},\mathbf{r}_0;n)+(\mathbf{r}'-\mathbf{r})\cdot\nabla\nabla g(\mathbf{r},\mathbf{r}_0;n), \quad \mathbf{r}'\approx\mathbf{r}, \tag{A18}$$

$$\nabla' g_1 \approx \nabla' g(\mathbf{r},\mathbf{r}';1)|_{\mathbf{r}'=\mathbf{r}_0} +(\mathbf{r}'-\mathbf{r}_0)\cdot\nabla\nabla g(\mathbf{r},\mathbf{r}_0;1), \quad \mathbf{r}'\approx\mathbf{r}_0. \tag{A19}$$

These expansions allow us to deal with singularities of higher order as compared to Eqs. (A12)–(A16). As an example we consider the term

$$\int_{\partial\delta V_n}(\hat{n}\nabla' g_1)\cdot(\nabla'\nabla' g_n)dS' = \int_{\partial\delta V_n}-\frac{\mathbf{R}'}{R'}[\nabla g(\mathbf{r},\mathbf{r}_0;1)+\mathbf{R}'\cdot\nabla\nabla g(\mathbf{r},\mathbf{r}_0;1)]\cdot k_0^2n^2\left(\mathbf{I}\left[\frac{i}{k_0nR'}-\frac{1}{k_0^2n^2R'^2}\right] -\frac{\mathbf{R}'}{R'}\frac{\mathbf{R}'}{R'}\left[\frac{3i}{k_0nR'}-\frac{3}{k_0^2n^2R'^2}\right]\right)g_n dS', \tag{A20}$$

where $\mathbf{R}'=\mathbf{r}'-\mathbf{r}_0$ and $R'=|\mathbf{r}'-\mathbf{r}_0|$. Some terms in Eq. (A20) can be immediately discarded because for the spherical exclusion volumes chosen here

$$\int_{\partial\delta V_n}\frac{\mathbf{R}'}{R'}dS=\mathbf{0}, \tag{A21}$$

$$\int_{\partial\delta V_n}\frac{\mathbf{R}'}{R'}\frac{\mathbf{R}'}{R'}\frac{\mathbf{R}'}{R'}dS=\mathbf{0}. \tag{A22}$$

This leaves us with the following:

$$\int_{\partial\delta V_n}(\hat{n}\nabla' g_1)\cdot(\nabla'\nabla' g_n)dS' = \int_{\partial\delta V_n}-\frac{\mathbf{R}'}{R'}\frac{\mathbf{R}'}{R'}\cdot[\nabla\nabla g(\mathbf{r},\mathbf{r}_0;1)]k_0^2n^2 \cdot\left(\mathbf{I}\left[-\frac{1}{k_0^2n^2}\right]-\frac{\mathbf{R}'}{R'}\frac{\mathbf{R}'}{R'}\left[-\frac{3}{k_0^2n^2}\right]\right)\frac{1}{4\pi}\frac{1}{R'^2}dS' = \frac{1}{3}\nabla\nabla g(\mathbf{r},\mathbf{r}_0;1)-3\nabla\nabla g(\mathbf{r},\mathbf{r}_0;1):\mathbf{M}, \tag{A23}$$

where

$$\mathbf{M}=\int_{\partial\delta V_n}\frac{\mathbf{R}'}{R'}\frac{\mathbf{R}'}{R'}\frac{\mathbf{R}'}{R'}\frac{\mathbf{R}'}{R'}\frac{1}{R'^2}\frac{1}{4\pi}dS' \tag{A24}$$

is a compound of four vectors grouped together or two dyadics grouped together. The symbol : is a double dot product such that for vectors $\mathbf{v}_1$, $\mathbf{v}_2$, $\mathbf{v}_3$, $\mathbf{v}_4$,

$$(\mathbf{v}_1\mathbf{v}_2):(\mathbf{v}_3\mathbf{v}_4)=(\mathbf{v}_2\cdot\mathbf{v}_3)(\mathbf{v}_1\cdot\mathbf{v}_4). \tag{A25}$$

In a similar way we obtain

$$\int_{\partial\delta V_n}(\hat{n}\cdot\boldsymbol{\nabla}' g_1)(\boldsymbol{\nabla}'\boldsymbol{\nabla}' g_n)dS' = \frac{1}{3}\nabla^2 g(\mathbf{r},\mathbf{r}_0;1)\mathbf{I} - 3\boldsymbol{\nabla}\boldsymbol{\nabla} g(\mathbf{r},\mathbf{r}_0;1):\mathbf{M}, \tag{A26}$$

$$\int_{\partial\delta V_1}(\hat{n}\cdot\boldsymbol{\nabla}' g_n)(\boldsymbol{\nabla}'\boldsymbol{\nabla}' g_1)dS' = \frac{1}{3}\nabla^2 g(\mathbf{r},\mathbf{r}_0;n)\mathbf{I} - 3\boldsymbol{\nabla}\boldsymbol{\nabla} g(\mathbf{r},\mathbf{r}_0;n):\mathbf{M}, \tag{A27}$$

where we have used

$$(\boldsymbol{\nabla}\boldsymbol{\nabla} g):\mathbf{II} = \nabla^2 g\mathbf{I}. \tag{A28}$$

The last term to consider in detail is

$$\int_{\partial\delta V_1} g_n\hat{n}\cdot(\boldsymbol{\nabla}'\boldsymbol{\nabla}'\boldsymbol{\nabla}' g_1)dS' \approx \int_{\partial\delta V_1}\Big[g(\mathbf{r},\mathbf{r}_0;n) + (\mathbf{r}'-\mathbf{r})\cdot\boldsymbol{\nabla} g(\mathbf{r},\mathbf{r}_0;n) + \frac{1}{2}(\mathbf{r}'-\mathbf{r})\cdot(\boldsymbol{\nabla}\boldsymbol{\nabla} g(\mathbf{r},\mathbf{r}_0;n))\cdot(\mathbf{r}'-\mathbf{r})\Big] \times\hat{n}\cdot(\boldsymbol{\nabla}'\boldsymbol{\nabla}'\boldsymbol{\nabla}' g_1)dS'. \tag{A29}$$

In this case only those terms in Eq. (A29) that are proportional to $g(\mathbf{r},\mathbf{r}_0;n)$ and $\boldsymbol{\nabla}\boldsymbol{\nabla} g(\mathbf{r},\mathbf{r}_0;n)$ are nonzero for the integration over the surface of the spherical exclusion volume δV_n. These nonzero terms are

$$g(\mathbf{r},\mathbf{r}_0;n)\int_{\partial\delta V_1}\hat{n}\cdot(\boldsymbol{\nabla}'\boldsymbol{\nabla}'\boldsymbol{\nabla}' g_1)dS' = -\frac{1}{3}k_0^2\mathbf{I}g(\mathbf{r},\mathbf{r}_0;n), \tag{A30}$$

$$\boldsymbol{\nabla}\boldsymbol{\nabla} g(\mathbf{r},\mathbf{r}_0;n):\int_{\partial\delta V_1}\frac{\mathbf{R}}{R}\frac{\mathbf{R}}{R}\hat{n}\cdot(\boldsymbol{\nabla}'\boldsymbol{\nabla}'\boldsymbol{\nabla}' g_1)dS' = -\nabla^2 g(\mathbf{r},\mathbf{r}_0;n)\mathbf{I} + 9\boldsymbol{\nabla}\boldsymbol{\nabla} g(\mathbf{r},\mathbf{r}_0;n):\mathbf{M}, \tag{A31}$$

where $\mathbf{R}=\mathbf{r}'-\mathbf{r}$. The above expressions can now be evaluated by use of the following property of the four vector compound $\mathbf{M}$:

$$\mathbf{A}:\mathbf{M} = \frac{1}{15}[\mathrm{Tr}(\mathbf{A})\mathbf{I} + \mathbf{A} + \mathbf{A}^T], \tag{A32}$$

where the dyadic $\mathbf{A}$ can be arbitrary. Here T refers to the transpose, and Tr refers to the trace or sum of diagonal elements. However, for the cases of interest here $\mathbf{A}$ will be the symmetric dyadic $\boldsymbol{\nabla}\boldsymbol{\nabla} g(\mathbf{r},\mathbf{r}_0;n)$ or $\boldsymbol{\nabla}\boldsymbol{\nabla} g(\mathbf{r},\mathbf{r}_0;1)$, and consequently the transpose operation will have no effect, i.e.,

$$(\boldsymbol{\nabla}\boldsymbol{\nabla} g):\mathbf{M} = \frac{1}{15}[\nabla^2 g\mathbf{I} + 2\boldsymbol{\nabla}\boldsymbol{\nabla} g]. \tag{A33}$$

After inserting the expressions (A12)–(A16), (A23), (A26), (A27), and (A29)–(A31) into Eq. (A11), adding the terms (A2), (A3) then finally by use of Eq. (A4) we obtain the main result of this appendix, namely,

$$\int_V \mathbf{G}(\mathbf{r},\mathbf{r}';1)k_0^2(n^2-1)\cdot\mathbf{G}(\mathbf{r}',\mathbf{r}_0;n)d^3r' = \mathbf{G}(\mathbf{r},\mathbf{r}_0;n) - \mathbf{G}(\mathbf{r},\mathbf{r}_0;1) + \frac{n^2-1}{k_0^2 n^2}\int_{\partial V}\Big((\hat{n}\boldsymbol{\nabla}' g_1)\cdot(\boldsymbol{\nabla}'\boldsymbol{\nabla}' g_n) - (\hat{n}\cdot\boldsymbol{\nabla}' g_1)(\boldsymbol{\nabla}'\boldsymbol{\nabla}' g_n) - \frac{n^2}{n^2-1}(\hat{n}\cdot\boldsymbol{\nabla}' g_n)(\boldsymbol{\nabla}'\boldsymbol{\nabla}' g_1) + \frac{n^2}{n^2-1}g_n(\hat{n}\cdot\boldsymbol{\nabla}')(\boldsymbol{\nabla}'\boldsymbol{\nabla}' g_1) - \mathbf{I}k_0^2\frac{n^2}{n^2-1}(g_1\hat{n}\cdot\boldsymbol{\nabla}' g_n - g_n\hat{n}\cdot\boldsymbol{\nabla}' g_1)\Big)dS'. \tag{A34}$$

Thereby we see that the volume integral expression for $\mathbf{G}^b$ has now been transformed into a surface integral, where the integral can be a surface far away from the Green's tensor singularities. Clearly $\mathbf{G}^b$ and $\mathbf{E}^b$ are nonsingular. The expression (A34) refers to the case where both positions $\mathbf{r}$ and $\mathbf{r}_0$ are inside the volume V. In the case where $\mathbf{r}$ is outside the volume V the only difference will be that the term $\mathbf{G}(\mathbf{r},\mathbf{r}_0;n)$ in Eq. (A34) should be omitted. The results Eqs. (15)–(17) are now directly obtained from Eq. (A1) and Eq. (A34).

Note that for the case of absorbing media, or passive media when the retarded Green's function is considered, the Green's functions decay exponentially with distance for large distances. Therefore, if we consider a volume with refractive index n taking up the whole three-dimensional space, and the surface of V is therefore placed at infinity, the surface integral in Eq. (A34) vanishes. In that case we are left with the following simple integral equation relation between two Green's tensors for different homogeneous media:

$$\mathbf{G}(\mathbf{r},\mathbf{r}_0;n)=\mathbf{G}(\mathbf{r},\mathbf{r}_0;1)+\int \mathbf{G}(\mathbf{r},\mathbf{r}';1)k_0^2(n^2-1)\cdot\mathbf{G}(\mathbf{r}',\mathbf{r}_0;n)d^3r'. \quad \text{(A35)}$$

*FAX: + 45 98 15 65 02; Email address: ts@mmphotons.dk
†FAX: + 45 45 93 65 81; Email address: bt@com.dtu.dk

[1] E. Purcell and C. Pennypacker, Astrophys. J. **186**, 706 (1973).
[2] B. Draine, Astrophys. J. **848**, 1988 (1988).
[3] A. Hoekstra, J. Rahola, and P. Sloot, Appl. Opt. **37**, 8482 (1998).
[4] G. Goedecke and S. O'Brien, Appl. Opt. **27**, 2431 (1988).
[5] M. Iskander, H. Chen, and J. Penner, Appl. Opt. **28**, 3083 (1989).
[6] C. Girard and A. Dereux, Rep. Prog. Phys. **59**, 657 (1996).
[7] O.J.F. Martin, C. Girard, D.R. Smith, and S. Schultz, Phys. Rev. Lett. **82**, 315 (1999).
[8] C. Girard, C. Joachim, and S. Gauthier, Rep. Prog. Phys. **63**, 893 (2000).
[9] D. Mulin, C. Girard, G. Colas Des Francs, M. Spajer, and D. Courjon, J. Microsc. **202**, 110 (2001).
[10] J.-C. Weeber, C. Girard, J.R. Krenn, A. Dereux, and J.-P. Goudonnet, J. Appl. Phys. **86**, 2576 (1999).
[11] C. Girard, A. Dereux, and C. Joachim, Phys. Rev. E **59**, 6097 (1999).
[12] A. Yaghjian, Proc. IEEE **68**, 243 (1980).
[13] M.L.M. Balistreri, J.P. Korterik, L. Kuipers, and N.F. van Hulst, Phys. Rev. Lett. **85**, 294 (2000).
[14] P. Phillips, J. Knight, B. Mangan, P. Russell, M. Charlton, and G. Parker, J. Appl. Phys. **85**, 6337 (1999).
[15] S.I. Bozhevolnyi, J. Erland, K. Leosson, P.M.W. Skovgaard, and J.M. Hvam, Phys. Rev. Lett. **86**, 3008 (2001).
[16] R. Chang and A. Campillo, *Optical Processes in Microcavities* (World Scientific, Singapore, 1996).
[17] H. Yokoyama and K. Ujihara, *Spontaneous Emission and Laser Oscillations in Microcavities* (CRC Press, New York, 1995).
[18] S. Ho, S. McCall, and R. Slusher, Opt. Lett. **18**, 909 (1993).
[19] D. Chu and S.-T. Ho, J. Opt. Soc. Am. B **10**, 381 (1993).
[20] M. Barnett, B. Huttner, R. Loudon, and R. Matloob, J. Phys. B **29**, 3763 (1996).
[21] M.S. Tomaŝ, Phys. Rev. A **51**, 2545 (1995).
[22] M.S. Yeung and T.K. Gustafson, Phys. Rev. A **54**, 5227 (1996).
[23] G. Björk, S. Machida, Y. Yamamoto, and K. Igeta, Phys. Rev. A **44**, 669 (1991).
[24] H. Rigneault, S. Robert, C. Begon, B. Jacquier, and P. Moretti, Phys. Rev. A **55**, 1497 (1997).
[25] H.P. Urbach and G.L.J.A. Rikken, Phys. Rev. A **57**, 3913 (1998).
[26] S. Ching, H. Lai, and K. Young, J. Opt. Soc. Am. B **4**, 2004 (1987).
[27] S. Ching, H. Lai, and K. Young, J. Opt. Soc. Am. B **4**, 1995 (1987).
[28] I. Abram, I. Robert, and R. Kuszelewicz, IEEE J. Quantum Electron. **34**, 71 (1998).
[29] T. Søndergaard and B. Tromborg, Phys. Rev. A **64**, 033812 (2001).
[30] C. Hooijer, D. Lenstra, and A. Lagendijk, Opt. Lett. **25**, 1666 (2000).
[31] W. Zakowicz and M. Janowicz, Phys. Rev. A **62**, 013820 (2000).
[32] E. Purcell, Phys. Rev. **69**, 681 (1946).
[33] T. Søndergaard, D. Lenstra, and B. Tromborg, Opt. Lett. **26**, 1705 (2001).
[34] J. v. Bladel, *Singular Electromagnetic Fields and Sources* (IEEE Press, NJ, 1991).
[35] O.J.F. Martin, C. Girard, and A. Dereux, Phys. Rev. Lett. **74**, 526 (1995).
[36] J. Nachamkin, IEEE Trans. Antennas Propag. **38**, 919 (1990).
[37] J.-M. Gérard and B. Gayral, IEEE J. Lightwave Technol. **17**, 2089 (1999).
[38] J.-M. Gérard, B. Sermage, B. Gayral, B. Legrand, E. Costard, and V. Thierry-Mieg, Phys. Rev. Lett. **81**, 1110 (1998).
[39] L. Graham, D. Huffaker, and D. Deppe, Appl. Phys. Lett. **74**, 2408 (1999).
[40] H. Nha and W. Jhe, Phys. Rev. A **54**, 3505 (1996).